

Oblique-incidence absorption spectroscopy studies of the plasmon in potassium halides

Arisato Ejiri

Department of Pure and Applied Sciences, University of Tokyo, 3-8-1 Komaba, Meguro-ku, Tokyo 153, Japan

(Received 28 May 1986; revised manuscript received 15 May 1987)

In the three potassium halides KCl, KBr, and KI, longitudinal excitations are precisely studied by the method of oblique-incidence absorption spectroscopy (OIAS) in the vacuum ultraviolet (10–20 eV) utilizing synchrotron radiation as a light source. Transverse absorption spectra of the halides are also observed in this energy region for comparison. A differential transmission ratio (DTR) of linearly polarized radiation is derived from the OIAS studies. In it, a longitudinal absorption appears as a positive peak and a transverse absorption as a negative one. The DTR spectra of these halides clearly show a prominent positive peak which has been ascribed to the plasmon. These results confirm the previous ones also measured by the present author. Several fine features superimposed on the plasmon peak are well resolved. The profiles of the plasmon peaks could be accurately analyzed by using the Lorentz model. The fine structure of the plasmon peak is successfully interpreted in terms of longitudinal-transverse splittings of a large transverse absorption peak and several fine structures on it in these halides.

I. INTRODUCTION

It is well known that, at photon energies higher than the exciton region in the fundamental absorption spectra of potassium halides, there exists a large and rather broad absorption band.^{1–6} The broad band has been interpreted in terms of interband transitions from the valence band to the upper conduction band⁷ or of the bound electron-polaron complex.⁸ This energy region is also known as the plasmon region because a large longitudinal excitation peak has been detected there by many optical measurements of dielectric parameters^{1–3,6} as well as by electron-energy-loss (EEL) experiments.^{9–14} The longitudinal peak is located at a little higher energy than that of the transverse absorption band and has commonly been interpreted in terms of a plasmon.⁹ The electron-polaron model⁸ has also predicted the existence of a longitudinal polaron absorption there.

Oblique-incidence absorption spectroscopy (OIAS) using linearly polarized radiation is well known as a powerful tool to detect longitudinal excitation in homogeneous substances.^{15,16} Successful applications of OIAS to studies of longitudinal electronic excitation in alkali halides were performed by the present author^{16–19} for the first time. Longitudinal excitons in several alkali halides were well demonstrated^{16,19,20} by OIAS with better resolution than that of EEL experiments.^{9–14} In the previous OIAS study of the plasmon in potassium halides,¹⁷ the differential transmission ratio (DTR) for *s* and *p* waves was successfully introduced by the present author. The DTR, $\Delta T/T_s$, where $\Delta T = T_s - T_p$, and T_s and T_p are *s*-wave transmittance and *p*-wave transmittance, respectively, in the oblique-incident configuration, shows longitudinal excitations as positive peaks and transverse as negative peaks. The plasmon was observed as a prominent positive peak in the DTR spectra. The

plasmon peak reproduced well the loss function (LF) peak derived from optical measurements and the EEL peak in their gross features and energies. Furthermore, several fine structures superimposed on the broad plasmon peak have been found in KCl in the previous study.¹⁷ Two or three substructures superimposed on the plasmon peak of K halides have already been found in the EEL^{10–14} and in the LF^{1–3,6,21} optically derived by other authors, but those fine structures have not been resolved completely because of poorer resolution in those measurements. The present author has interpreted these fine structures in terms of longitudinal excitons since they well correspond energetically to the three peaks which had been found by Piacentini *et al.*²² in their thermo-modulated-energy loss experiment of KCl and proposed as longitudinal excitons by them.

The present studies are intended to measure the DTR of plasmon loss more accurately in KCl, KBr, and KI, and to improve the resolution of previous results by the use of vuv synchrotron radiation from the electron synchrotron (INS-ES, Institute for Nuclear Study, Tokyo) as a continuum polarized light source. An attempt is made to analyze the DTR spectra as well as that of LF with a Lorentz oscillator model. Accurate spectra of transverse absorption in this region will be also demonstrated since they are necessary for comparison with an analysis of the longitudinal spectra.

II. EXPERIMENTAL PROCEDURE

Oblique-incidence amplitude transmittance of a plane parallel thin film specimen is given from the classical electromagnetic theory as²³

$$t = \frac{t_1 t_2 \exp(i\hat{\delta})}{1 + r_1 r_2 \exp(2i\hat{\delta})}, \quad (1)$$

where (r_1, t_1) and (r_2, t_2) are the Fresnel coefficients for the first and second surfaces of the film, and $\hat{\delta}$ is a factor including attenuation and phase shift within the film.

When the Fresnel coefficients for p and s waves are

$$t_p = \frac{2\hat{\epsilon}(\hat{\epsilon} - \sin^2\theta)^{1/2} \cos\theta}{2\hat{\epsilon}(\hat{\epsilon} - \sin^2\theta)^{1/2} \cos\theta \cos\hat{\delta} - i(\hat{\epsilon}^2 \cos^2\theta + \hat{\epsilon} - \sin^2\theta) \sin\hat{\delta}}, \quad (2)$$

$$t_s = \frac{2(\hat{\epsilon} - \sin^2\theta)^{1/2} \cos\theta}{2(\hat{\epsilon} - \sin^2\theta)^{1/2} \cos\theta \cos\hat{\delta} - i(\hat{\epsilon} + 1 - 2\sin^2\theta) \sin\hat{\delta}},$$

where θ is the angle of incidence, and $\hat{\epsilon} (= \epsilon_1 + i\epsilon_2)$ is the frequency-dependent dielectric function. $\hat{\delta}$ is given by

$$\hat{\delta} = (2\pi d/\lambda)(\hat{\epsilon} - \sin^2\theta)^{1/2},$$

where d is the thickness of the film and λ is the wavelength of the radiation.

The intensity transmittances for p waves, T_p , and for s waves, T_s , are given by $T_p = |t_p|^2$ and $T_s = |t_s|^2$. On the assumption of $2\pi d \ll \lambda$, an approximate relation for the differential transmission ratio (DTR), $\Delta T/T_s$, was derived by the present author in the form^{16,17}

$$\Delta T/T \approx \frac{\delta \sin^2\theta}{\cos\theta} \left[\frac{\epsilon_2}{\epsilon_1^2 + \epsilon_2^2} - \epsilon_2 \right], \quad (3)$$

where $\delta = 2\pi d/\lambda$.

Equation (3) indicates that longitudinal excitations are detectable directly by an oblique-incidence optical measurement on a thin-film specimen, even of an isotropic substance and that they appear as positive peaks in the DTR spectrum. It means that a specimen having a finite thickness much less than the wavelength of light plays the role of a specimen having an anisotropy in its normal direction for oblique-incident p waves.

The ratio of transmittances T_p/T_s was directly measured by using a sample chamber rotatable around the axis of the incident radiation in the photon energy region of 10–20 eV. The angle of incidence can be varied from outside the vacuum by rotating specimen around an axis perpendicular to the incident radiation. The thin-film specimen was deposited on a collodion (cellulose nitrate) thin-film substrate by evaporation in vacuum. The thickness of each thin-film specimen was measured with a calibrated quartz thickness monitor. Details of the procedure for sample preparation are identical with those of the previous work,¹⁷ but the present measurement was done *in situ* after the deposition at room temperature. It has already been confirmed¹⁷ that the collodion substrate is insensitive to the polarization direction of incident radiation. A vertical dispersion type VUV monochromator,²⁵ which was newly constructed and designed to enhance the polarization of synchrotron radiation and to have a high throughput and resolution, was utilized for this measurement. Resolution was kept at 1 Å during the measurement. A Bendix 306 electromagnetic-type photomultiplier was used as a

used, Eq. (1) becomes the amplitude transmittance coefficients for p and s waves, t_p and t_s , respectively, given by²⁴

photon detector. The degree of polarization of the synchrotron radiation emerging from the exit slit is shown in Fig. 1.²⁵ Correction of the observed DTR spectra for partial polarization of radiation was not performed because a degree of polarization higher than 90% is achieved in the photon energy region on the present measurement.

In the present photon energy region, transverse absorption spectra of these halides for normal incidence were also measured separately from the oblique-incidence measurement for similar but different specimens by using an ordinary 50 cm Seya-Namioka monochromator, the resolution of which was kept at 3 Å during the measurement.²⁶ The measurements were also performed *in situ* after deposition of the specimens. The thickness of the specimens was not measured accurately. The effects of the substrate on absorption spectra were compensated with signals from radiation passing through an undeposited substrate. The synchrotron radiation was also used as a light source, and a windowless Be-Cu photomultiplier was utilized as a detector in this measurement. Optical density curves of KCl, KBr, and KI at room temperature (RT) and at liquid-nitrogen temperature (LNT) were obtained.

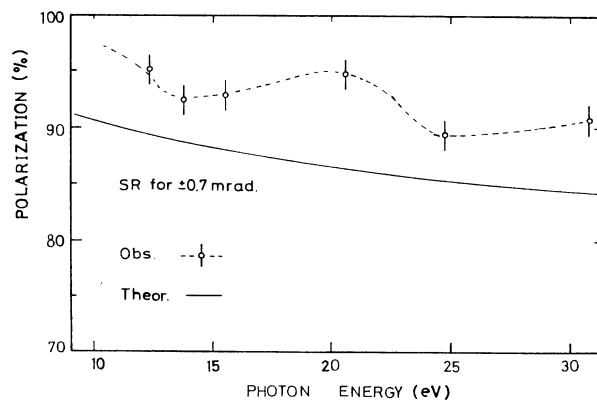


FIG. 1. Polarization of the synchrotron radiation (SR) used for ± 0.7 mrad to the orbital plane. Observed values are of the radiation emerging from the exit slit of the monochromator, and theoretical curve is of the original SR.

III. RESULTS AND DISCUSSIONS

A. KCl

1. Experimental results

DTR, $\Delta T/T_s$, spectra obtained in KCl at angles of incidence 30° , 45° , and 60° are shown in Fig. 2.²⁰ Normal incidence transverse absorption spectra obtained at RT and LNT are indicated in Fig. 3. The transverse absorption peak around 13 eV at RT is also shown in Fig. 2 for comparison. The present absorption spectrum at LNT shown in Fig. 3 is connected with the low-lying excitonic spectrum which is referred to the results of Eby *et al.*²⁷ in the same optical density scale for comparison of intensity. The observed large absorption peak at 13 eV not only has an intensity comparable with the first exciton as well as with the second one (peak c of Fig. 3) but also has a large width and three shoulders (*e*, *f*, *g*). Peak *d* and shoulders *e* and *f* show a large enhancement upon cooling, whereas shoulder *g* does not vary. A curve of the joint density of states that has been theoretically derived by Overhof⁷ without taking exciton effects into account is also indicated in Fig. 3. From the comparison between the experimental spectra and the theoretical curve, excitonic transitions also seem to contribute to the absorption spectrum in the 12–14 eV region. The DTR spectra shown in Fig. 2 have a broad peak around 14 eV that becomes more prominent as the angle of incidence increases. Five fine structures, *A–E*, are superimposed on the peak, and a shoulder *A* (12.4 eV) and peaks *D* (14.0 eV) and *E* (15.0 eV) become prominent at $\theta=45^\circ$ and 60° , whereas peak *B* (12.8 eV) is, however, more distinguishable in the spectra of $\theta=30^\circ$ and 45° . Peak *C* (13.3 eV) appears at all angles.

The broad positive peak and three fine structures (*C*, *D*, and *E*) refine and confirm our previous results,¹⁷ and

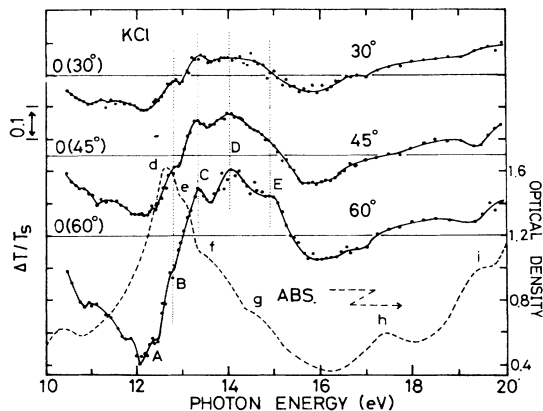


FIG. 2. DTR spectra (—) observed at angles of incidence, 30° , 45° , and 60° and transverse absorption spectrum (---) observed at room temperature in KCl. The latter is the same spectrum as the one shown in Fig. 3. Thickness of the film specimen used for DTR measurement is 200 Å. Fine structures corresponding to each other in these DTR spectra are connected by vertical dotted lines, respectively.

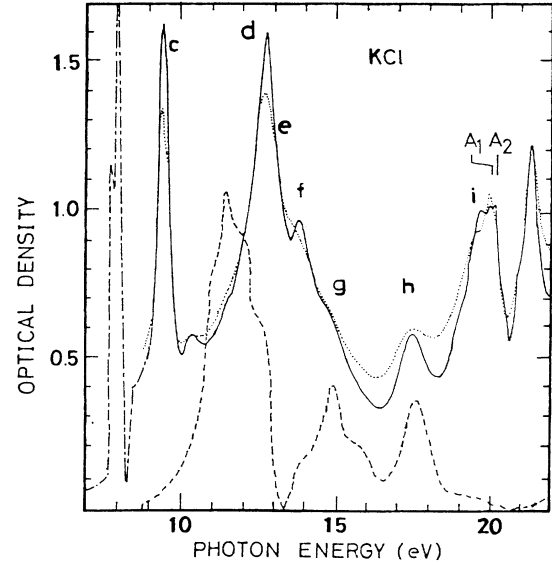


FIG. 3. Absorption spectra of KCl observed at room (· · ·) and liquid nitrogen (—) temperatures. A curve of the density of state (---) (Ref. 7) and the low-lying exciton peaks (- · - ·) (Ref. 27) are also illustrated for comparison. Peaks A_1 and A_2 are known as the doublet of K^+3p core exciton at the Γ point in Brillouin zone.

the shoulders *A* and *B* are found for the first time. The energies of these structures are listed and compared with data presented by other authors in Table I. The present DTR spectrum at $\theta=60^\circ$ is shown in Fig. 4 together with the LF spectrum obtained from dielectric analysis of optical reflection measurements by Stephan²¹ and with the result of EEL by Creutzburg.¹² Two shoulders can be seen on the EEL peak at both sides of the main peak. Similar structures are also seen on the LF peak. This comparison clearly indicates that the DTR spectrum reproduces well the other loss spectra and shows the best resolution of them and that the shoulders *A* and *B* are missed in the others.

2. Lorentz oscillator model

In order to reveal the details of the interrelation between the transverse and the longitudinal spectra, those spectra and the dielectric parameters are analyzed with Lorentz oscillator model. It is assumed that the absorption peak around 13 eV consists of resonance absorptions caused by several oscillators. Based on the model, dielectric parameters concerning the m oscillators in the real system are given by

$$\epsilon_T = \epsilon_0 - \sum_{n=1}^m \frac{\sigma_n}{E^2 - E_n^2 - iE\gamma_n}, \quad (4)$$

where ϵ_T is the total dielectric function and ϵ_0 the background value. E_n is the energy of the n th oscillator, and γ_n is its full width of half maximum. σ_n is proportional to its oscillator strength.

TABLE I. Energy positions of longitudinal transverse structures in KCl (in eV). Letters *mp*, *p*, and *s* mean a main peak, peak, and shoulder, respectively. Observed L-T splittings $\hbar\omega_{L-T}$ are indicated in the third column. Oscillators used in the Lorentz model fittings are also shown in the last column. Experimental and theoretical n_{eff} , $\hbar\omega_p$, and $\hbar\omega_{\text{obs}}$ are listed on the bottom.

Present study		$\hbar\omega_{L-T}$	Optical LF ^a	EEL ^b	TML ^c	Oscillators
Absorption (RT)	DTR					
	A 12.4 <i>s</i>					
<i>d</i> 12.7 <i>p</i>	B 12.8 <i>s</i>	0.1				12.5
<i>e</i> 13.1 <i>s</i>	C 13.3 <i>p</i>	0.2	13.2 <i>p</i>	13.2 <i>s</i>	13.35 <i>p</i>	13.1
<i>f</i> 13.8 <i>s</i>	D 14.0 <i>mp</i>	0.2	13.9 <i>p</i>	14.0 <i>p</i>	14.25 <i>p</i>	13.7
<i>g</i> 14.7 <i>s</i>	E 15.0 <i>p</i>	0.3	15.0 <i>s</i>	14.7 <i>s</i>	15.0 <i>p</i>	14.6
	n_{eff}		$\hbar\omega_p$	$\hbar\omega_{\text{obs}}$		
Experimental ^a	4.0			13.9		
Theoretical ^d	4.0		9.4	12.7		($\hbar\omega_g = 8.5$)
	6.0		11.6	14.4		

^aReferences 3 and 21.

^bReference 12.

^cReference 22.

^dReference 29.

One main oscillator and three subsidiary ones located on the upper side of the main oscillator are taken into account. The Lorentz model calculations to reproduce the observed absorption spectrum as well as the observed DTR spectra are performed by using Eqs. (1) and (2) with the total dielectric functions derived from Eq. (4) for the four-oscillator model. The calculated results, the best fit absorption peak and DTR spectra, use the parameters shown in Table II. The calculated DTR ($\theta = 60^\circ$) and optical density spectra for a specimen with thickness of 200 Å are compared with the corresponding experimental spectra in Fig. 5. Each of the calculated spectra reproduced well the profile and energy of experimental spectrum, respectively. Disagreement in intensi-

ties is, however, found between the experimental optical density and the calculated one. This may be mainly due to an error in the thickness of specimen. Another disagreement found in gross intensities between the experimental DTR peak and the calculated one may be mainly due to some influence of the substrate film.¹⁷ The present analysis, however, predominantly concentrates on obtaining coincidence of spectral profiles between the experiments and the calculations.

All calculated DTR, ϵ_2 , and loss function spectra are shown in Fig. 6. The four components of the ϵ_2 spectrum are also shown in the same figure as dotted lines. From the Lorentz model analysis, the following facts are confirmed. (1) A prominent positive peak on the DTR spectra and a loss function peak around 14 eV are ascribed to the oscillators located around 13 eV. (2) Each of the four fine structures on the DTR peak has its counterpart in the loss function at nearly the same energies, as can be seen in Fig. 6. (3) The fine structures on the DTR or on the loss function are caused by the presence of subsidiary oscillators located on the higher energy side of the main oscillator. In Fig. 6 a shoulder at 13.0 eV in DTR corresponds to the main oscillator peak (12.5 eV), and small peaks at 13.4, 14.0, and 14.8 eV in DTR correspond, respectively, to three shoulders which originate from the three subsidiary oscillators at 13.1, 13.7, and 14.6 eV. They indicate the longitudinal-transverse splittings of magnitudes 0.5, 0.3, 0.3, and 0.2

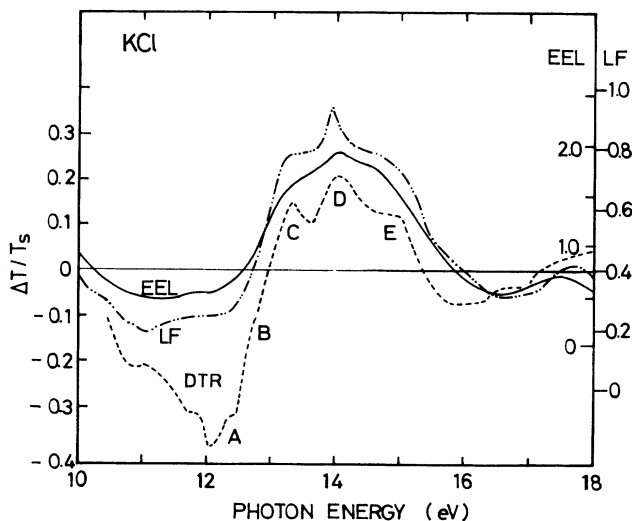


FIG. 4. The plasmon peaks in the present DTR spectrum at $\theta = 60^\circ$ (---), in the EEL (—) (Ref. 12) and in the LF (-·-·-) (Ref. 21) spectra.

TABLE II. Numerical parameters of the oscillators fitted to the observed spectra in KCl.

Oscillators	E (eV)	γ (eV)	σ	ϵ_0
1	12.5	1.0	15	
2	13.1	0.5	1.5	1.0
3	13.7	0.8	3.0	
4	14.6	1.0	2.0	

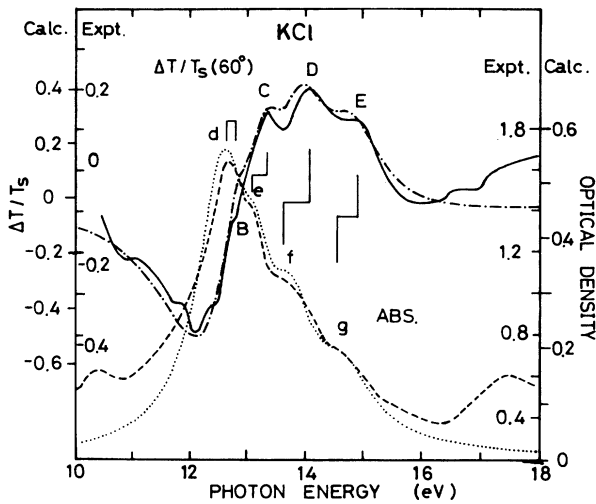


FIG. 5. Comparison between the experimental results and the Lorentz model calculations in KCl. DTR (60°); experimental, \cdots ; calculated, $-\cdots-$. Absorption spectra; experimental, $---$; calculated, $-\cdot-\cdot-$. Pairs of vertical lines indicate longitudinal-transverse pairs for the experimental results. Thickness of specimen is 200 \AA for both calculations and for the experimental DTR.

eV, respectively. In the Appendix the contributions of fine structure closely located on the higher energy side of a larger absorption peak to the loss function spectrum are generally examined with the Lorentz model.

By analogy with the Lorentz model analysis, it can be stated that the existence of the broad positive peak in

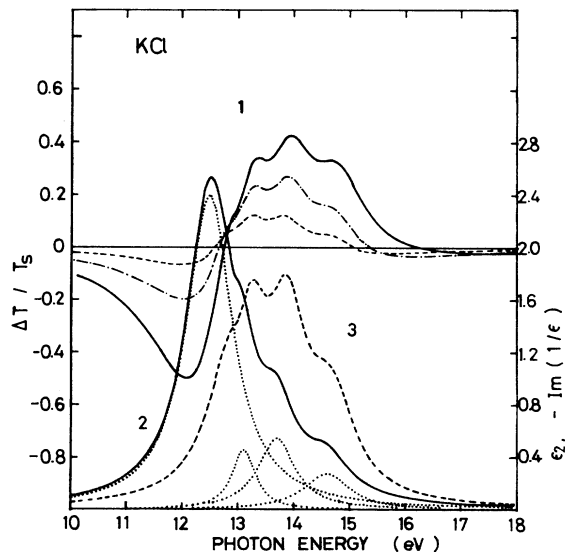


FIG. 6. Theoretical curves calculated from the multioscillator model fitted to the present experimental results of KCl. Curve 1 indicates three DTR spectra (\cdots , 30° ; $-\cdots-$, 45° ; $---$, 60°); curve 2 indicates the ϵ_2 spectrum which is divided into four components (\cdots); and curve 3 indicates the loss function ($---$). Numerical parameters used in the model are shown in Table II and the thickness of specimen for DTR spectra is 200 \AA .

DTR around 14 eV or the existence of the large loss function peak is essentially attributed to the existence of the large absorption band at about 13 eV and that the observed fine structures *B*, *C*, *D*, and *E* in the DTR spectra are corresponding longitudinal counterparts of the main absorption peak and of the three shoulders on its higher energy side. These longitudinal-transverse pairs are indicated by pairs of vertical lines in Fig. 5. The statements essentially support our previous proposal¹⁷ but improve the assignment of the longitudinal counterparts of the main absorption peak on shoulder *B* which was not found in the previous work. The present results tabulated in Table I improve also the previous proposal by Piacentini *et al.*²² who have incorrectly assigned a peak of the thermo-modulated energy loss corresponding to peak *C* to the longitudinal counterpart of the main absorption peak. The shoulder *A* and other structures on the DTR at energies lower than 12 eV are longitudinal counterparts of transverse structures on the lower energy side of the main absorption peak that are not our present concern.

In the present calculations of the Lorentz model mentioned above, the background dielectric parameter ϵ_0 has unity as the best choice. The ϵ_0 value which reflects the influence of electronic transitions other than the oscillators employed may, in fact, be complex. Several iterations of the best fitting calculation show the choice to be best with an allowance of ± 0.1 in both real and imaginary parts.

3. Discussions

It has already been confirmed by the present author that the positive peaks in the DTR spectra attributed to plasmon excitation for the following reasons.¹⁷ (1) Equation (3) indicates that a longitudinal excitation appears as a positive peak in the DTR spectra. (2) Exact calculation of DTR spectra by Eq. (2) utilizing available optical constants²⁸ in KCl shows a positive peak at the same energy as a loss function peak obtained with the same optical constants. Furthermore, the observed positive peak agrees well with the calculated positive peak and also with the peak of EEL experiment in its energy and gross feature. (3) The presence of such longitudinal absorption (plasmon) has theoretically been predicted by Horie²⁹ and Miyakawa.³⁰

Horie²⁹ has theoretically derived an approximate formula for the plasmon energy to be observed in insulators ($\hbar\omega_{\text{obs}}$) as

$$\omega_{\text{obs}}^2 \simeq \omega_g^2 + \omega_p^2, \quad (5)$$

where $\hbar\omega_g$ is band gap energy and $\hbar\omega_p$ is the free electron plasma energy. Subsequently, Miyakawa³⁰ has theoretically investigated interrelations among longitudinal excitons, Van Hove singularities, and the plasmon in alkali halides, and predicted the existence of the plasmon at the M_3 edge of the density of states. He has also derived an approximate expression for the plasmon energy

to be observed in alkali halides $\hbar\omega_{\text{app}}$ as

$$\omega_{\text{app}}^2 \simeq \omega_m^2 + \omega_p^2 (n_{\text{eff}}/n), \quad (6)$$

where ω_m is an average frequency of interband absorptions. By using the free electron plasmon $\hbar\omega_p = 11.6$ eV for $n = 6$ and the band gap energy $\hbar\omega_g = 8.5$ eV, Horie's predicted $\hbar\omega_{\text{obs}}$ becomes 14.4 eV from Eq. (5) which agrees very well with the experimental value of 14.1 eV. On the other hand, the effective number of electron n_{eff} exhausted at 14 eV in KCl is available from Stephan's work as about 4.0. Then $n = 6$ is too large to compare with the Stephan's value. This discrepancy may be also ascribed to the existence of the fine structure which shifts the plasmon appreciably to higher energy. Expressions (5) and (6) are very similar to each other but have different meanings in both terms on the right-hand side. If the experimental value 14.1 eV is put into $\hbar\omega_{\text{app}}$ in Eq. (6), the $\hbar\omega_m$ is derived as 10.4 eV by the use of the same $\hbar\omega_p$, $n_{\text{eff}} = 4.0$, and $n = 6$. The $\hbar\omega_m$ (10.4 eV) is located in the interband absorption region, but this expression gives a rather loose restriction. Thus, the present results seem to support essentially Miyakawa's theory, but the observed phenomena are complicated because of the existence of fine structures near the edge as seen in the above analysis. Then, the approximate expression derived by Miyakawa, in which the contribution from higher energy bands are assumed to be negligible, may not be utilized for numerical analysis of the plasmon energy. Therefore, Horie's values are indicated together with experimental results in Table II for comparison.

On the other hand, the bound electron polaron complex model, which consists of an electron and a hole, each dressed with virtual longitudinal excitons, has also been proposed theoretically for the longitudinal peak by Collins *et al.*⁸ In their work, the energy positions of the transverse peak are predicted with the model for several alkali halides. The predicted position for KCl (13.8 eV) is larger by 1 eV than the experimental value but that for KBr (11.7 eV) agrees well with the experiment. The polaron model, however, has not derived the energies of the longitudinal peak and has nothing to do with the observed fine structure on the longitudinal peak. Then, it is impossible to compare the model with the present experimental results of the longitudinal excitation.

Thus, it can be said that the positive peak of the DTR or the loss function peak in KCl is attributed to both the plasmon at the M_3 edge and excitons existing around the edge,²² and that the longitudinal modes of the latter contribute predominantly to the determination of the profile of the peak and appreciably to its shift toward the upper energy. Generally, the plasmon in alkali halides seems to appear just above the largest and prominent interband absorption peak, contrary to the plasmon in the free electronlike metals in which the plasmon appears at $\hbar\omega_p$ very far from the interband transition. This difference is due to a large difference in intensities of the interband transitions between alkali halides and metals, because the longitudinal-transverse (L-T) splitting is generally proportional to oscillator strength. If the prominent peak is absent, the plasmon does not appear near there as can be seen in the case of potassium fluoride.²¹

B. KBr

1. Experimental results

The observed DTR spectra in KBr at angles of incidence, 30°, 45°, and 60°, and the observed absorption spectra in KBr at RT and LNT are shown in Figs. 7 and 8, respectively. In Fig. 7 the absorption spectrum at RT is also shown for comparison. In Fig. 8 a curve of the joint density of states derived by Overhof⁷ and the results of Eby *et al.*²⁷ at the lower energy region are also illustrated in a similar manner with the case of KCl. The large absorption peak around 12 eV has a comparable height with low-lying exciton peaks and has a much greater width composed of several fine structures (*d-i*). Peak *f* and shoulders *g*, *h*, and *i* are remarkably enhanced upon cooling. Although the curve of the joint density of states shows that the large peak predominantly consists of interband transitions, contributions of several excitonic transitions to the absorption peak seem to exist in the 12–14 eV region. The DTR spectra in Fig. 7 have a prominent positive peak around 13 eV. Several fine structures are superimposed on the positive peak and are indicated by *A*, *B*, *C*, *D*, and *E* on the 60° spectrum.

The observation of the prominent positive peak in the higher energy region of the large absorption peak confirms the previous results¹⁷ obtained by the present author in KBr similarly to the case of KCl. This means that the positive peak corresponds to the LF peak derived by other authors^{1,3} and also to the results of EEL

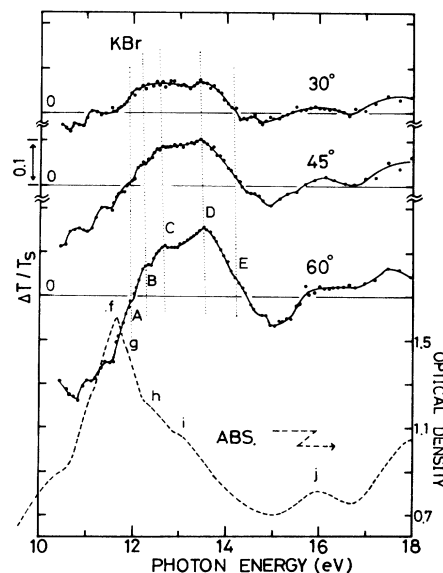


FIG. 7. DTR spectra (—) observed at angles of incidence, 30°, 45°, and 60° and transverse absorption spectrum (---) observed at room temperature in KBr. The latter is the same spectrum as the one shown in Fig. 8. Thickness of the film specimen used in the DTR experiment in 170 Å. Fine structures corresponding to each other in these DTR spectra are connected by vertical dotted lines, respectively.

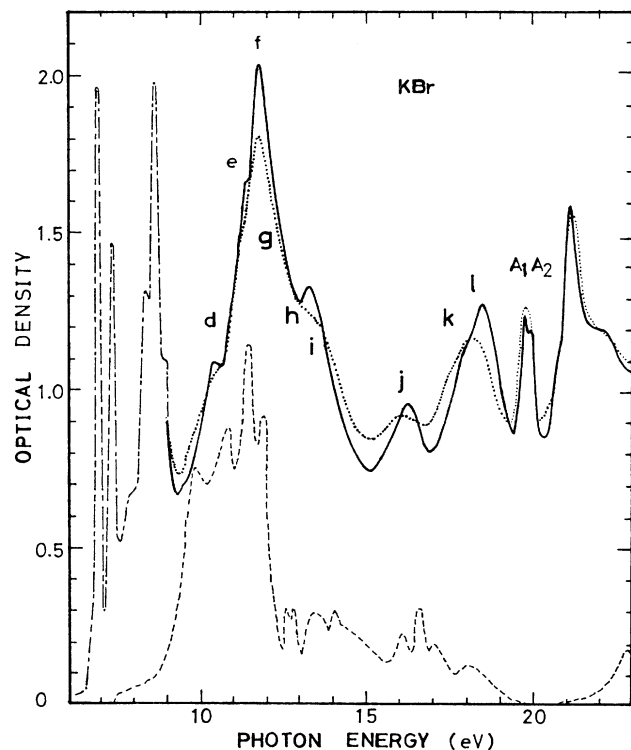


FIG. 8. Absorption spectra of KBr observed at room (—) and liquid-nitrogen (---) temperatures. A curve of the density of state (· · · ·) (Ref. 7) and the low-lying exciton peaks (— · — ·) (Ref. 27) are also illustrated for comparison. Peaks A_1 and A_2 are well known⁴ as the K^+3p core exciton at the Γ point in BZ.

experiments.^{11,12} The fine structures observed on the positive peak, however, differ from the previous results obtained by the present author,¹⁷ and improve them appreciably.

2. Discussions

Transverse absorption and the DTR spectra for a thin-film specimen are exactly calculated using Eq. (2) and the optical constants in KBr derived by Stephan.²¹ The results of the calculations and the LF spectrum obtained by Stephan are shown in Fig. 9. It is also confirmed for KBr from the calculations that a positive peak in the DTR spectra and the LF peak, both of which are calculated with the same optical constants, have a similar profile in each other as the case of KCl.

Previous work on the LF by Stephan³ and the EEL experiment by Keil¹¹ are compared with the present DTR experimental result in Fig. 10. The present experiment shows the best resolution of them and resolves the small shoulder *A*. Thus, the analysis of the DTR spectra with the Lorentz oscillator model becomes possible and effective.

The four-oscillator fit using the parameters in Table III produces comparable agreements with the KBr data as in the case of KCl, which was shown in Figs. 5 and 6.

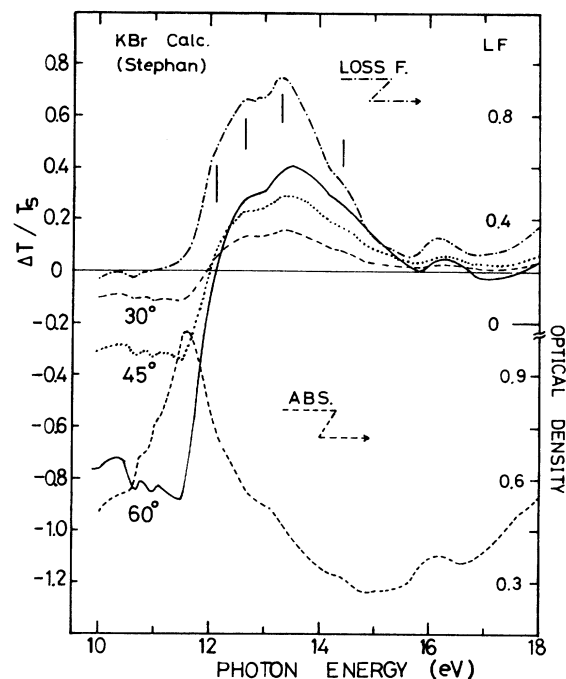


FIG. 9. DTR's (---, 30°; · · · · 45°; —, 60°) and LF (— · — ·) in upper part, and absorption spectrum (---) in lower part calculated by using the available optical constants of KBr (Ref. 21) for a thin film of 200 Å in thickness.

Also found from the Lorentz model analysis of KBr as in the case of KCl, that the positive peak in the DTR spectra is essentially caused by the presence of the large absorption peak, but its profile is predominantly influenced by the presence of the small subsidiary structures on the absorption spectrum and that the observed fine peaks *B*, *C*, and *D* on the DTR are just the longitudinal counterparts of the three shoulders located on the

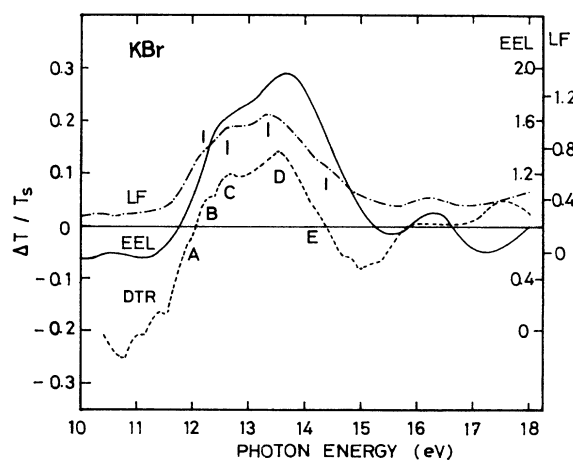


FIG. 10. The plasmon peaks in the present DTR spectrum at $\theta=60^\circ$ (---) in the EEL (—) (Ref. 11) and in the LF (— · — ·) (Ref. 3) spectra.

TABLE III. Numerical parameters of the oscillators fitted to the observed spectra in KBr.

Oscillators	E (eV)	γ (eV)	σ	ϵ_0
1	11.5	0.8	18	1.0
2	11.9	0.7	2	
3	12.5	0.7	2	
4	13.2	1.0	3	

upper side of the main absorption peak (g , h , i), respectively, and the shoulder A is the counterpart of the main peak. The results of the present work in KBr are listed in Table IV together with those of previous works.

The present results qualitatively support the Miyakawa's theory³⁰ which has predicted the existence of a plasmon at an M_3 edge of the density of states. On the other hand, Horie's theoretical value²⁹ of $\hbar\omega_{\text{obs}}$ becomes 13.3 eV by using the band gap energy $\hbar\omega_g = 7.8$ eV and $\hbar\omega_p = 10.7$ eV for $n = 6$. This value is very close to the present result of about 13.5 eV. However, effective number of electron n_{eff} exhausted at about 13 eV in KBr is available from Stephan's work²¹ as about 4.5. This discrepancy also resembles the case of KCl.

In this way, the situation in KBr is very similar to that of KCl. Thus, it can be also stated that the positive peak of the DTR or the loss function peak in KBr is attributed to both plasmon loss at the M_3 edge and the excitons existing around the edge and that the longitudinal modes of the excitons contribute predominantly to the determination of the profile of the broad positive peak and appreciably to its shift toward upper energy.

C. KI

1. Experimental results

The present results of the DTR spectra are shown in Fig. 11. The DTR spectra of KI are observed for the first time, although they are limited to 10 eV as a lower limit to the energy. On the DTR spectra, a broad posi-

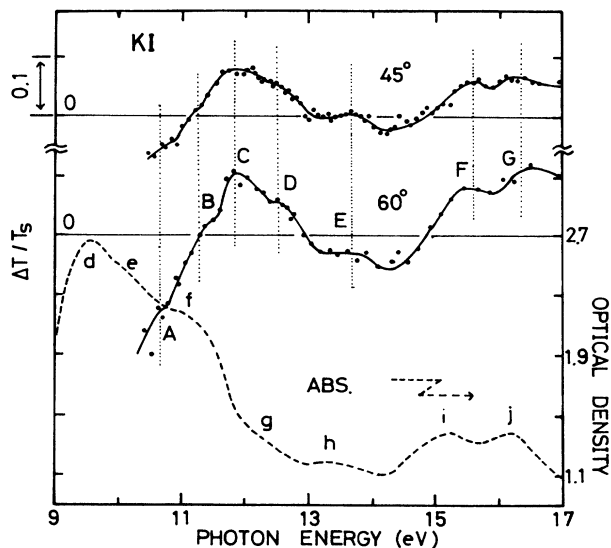


FIG. 11. DTR spectra (\dashrightarrow) at angles of incidence, 45° and 60°, and transverse absorption spectrum ($---$) observed at room temperature in KI. The latter is the same spectrum as the one shown in Fig. 12. Thickness of the film specimen used for DTR measurement is about 200 Å. Fine structures corresponding to each other in the DTR spectra are connected with vertically dotted lines, respectively.

tive peak appears at around 12 eV. Four fine structures A , B , C , and D are superimposed on the positive peak. Other small peaks E , F , and G are also observed clearly at high energy region.

In Fig. 12 the absorption spectra obtained at RT and LNT are shown and compared with the joint density of states obtained by Overhof⁷ and with the results obtained by Eby *et al.*²⁷ in the same manner with the cases of KCl and KBr. A large absorption band around 10 eV has a much lower height than the exciton peaks at the interband threshold and has an appreciably greater

TABLE IV. Energy positions of longitudinal and transverse structures in KBr (in eV). Letters in the table similarly mean those in the Table I.

Absorption	Present study		Optical LF ^a	EEL ^b	Oscillators
	DTR	$\hbar\omega_{\text{LT}}$			
f 11.7 p	A 12.0 s	0.3			11.5
g 12.0 s	B 12.3 p	0.3	12.2 s		11.9
h 12.4 s	C 12.6 p	0.2	12.6 p	12.6 s	12.5
i 13.1 s	D 13.5 mp	0.4	13.4 p	13.7 p	13.2
	n_{eff}	$\hbar\omega_p$		$\hbar\omega_{\text{obs}}$	
Experimental ^a	4.5			12.6	
Theoretical ^c	4.5	9.3		12.1	($\hbar\omega_g = 7.8$)
	6.0	10.7		13.3	

^aReference 21.

^bReference 11.

^cReference 29.

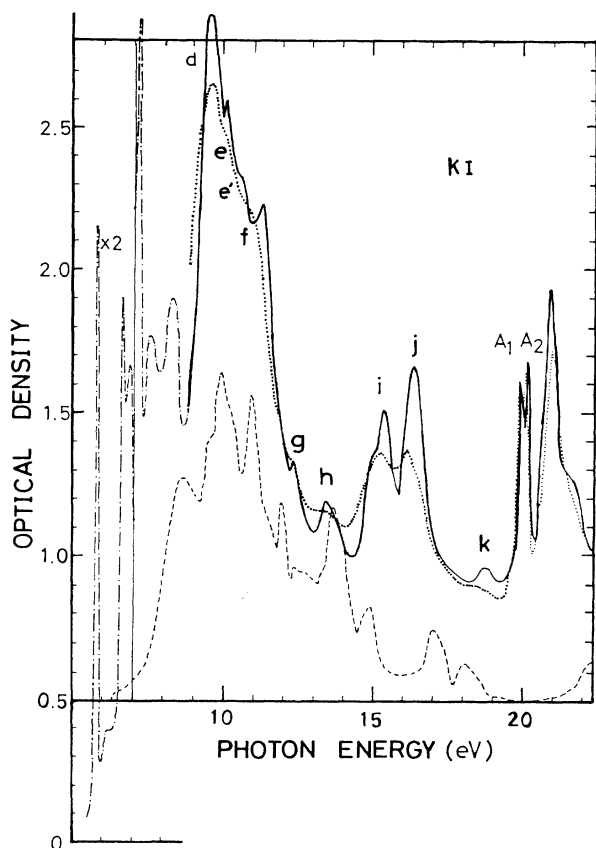


FIG. 12. Absorption spectra of KI observed at room (· · · ·) and liquid nitrogen (—) temperatures. A curve of the density of state (— — —) (Ref. 7) and the low-lying exciton peaks (— · — · —) (Ref. 27) are also illustrated for comparison. Peaks A_1 and A_2 are known (Ref. 4) as the doublet of K^+3p core exciton at the Γ point in BZ.

width being composed of several fine structures ($d-h$). The calculated joint density of states⁷ seems to reproduce the experimental peak in its energy and fine structures in the 9–15 eV region, but the experimental curves are rather complicated around the 9–11 eV region. The fine structures e , f , and g on the absorption peak show remarkable temperature effects of enhancement and blue shifts upon cooling, whereas the main peak d shows no such effects. Another shoulder e' also appears between e and f only in the LNT spectrum. The absorption spectrum at RT is also illustrated in Fig. 11 in the energy range of 9–17 eV for comparison with the DTR spectra.

2. Discussions

The present experimental DTR spectrum at 60° is compared with the previous EEL experiment by Creutzburg¹² in Fig. 13. The loss function spectrum derived from optical measurement is not available. The present DTR peak around 12 eV shows good resolution and reveals the existence of four fine structures, whereas the EEL peak is rather broad but indicates two shoul-

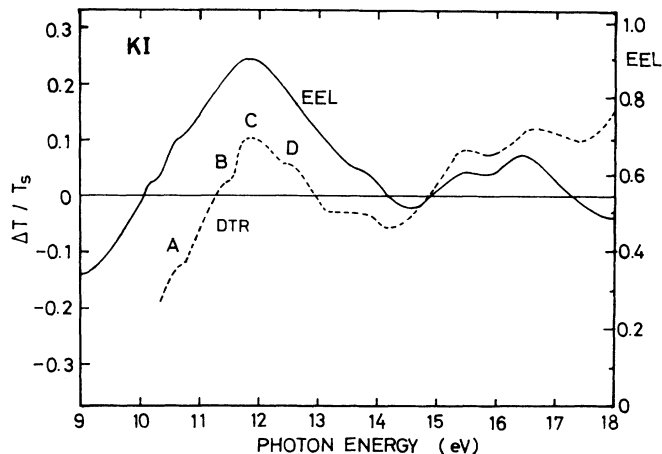


FIG. 13. The plasmon peaks in the present DTR spectrum at $\theta=60^\circ$ (— — —) and in the EEL (—) (Ref. 12) spectrum of KI.

ders between 10 and 11 eV. The upper of the two shoulders coincides with shoulder A (10.7 eV) on the DTR peak, but the lower one is beyond the present measurements. The present numerical results are compared with the work of other authors in Table V.

Five oscillators are employed in the Lorentz model analysis of the experimental results in KI. Best-fit calculation which reproduce the experimental absorption spectrum and DTR spectra use the numerical parameters shown in Table VI. The ϵ_0 is chosen as $1.0+0.1i$ in the fitting process. The calculated DTR ($\theta=60^\circ$) for a specimen with thickness of 150 Å and the calculated optical density spectrum for a specimen of 600 Å are compared with the corresponding experimental results in Fig. 14. As can be seen in the figure, the profile of the calculated DTR spectrum reproduces well that of the experimental one. Also, the calculated optical density reproduces very well the experimental spectrum in the energy positions of the fine structures and in the intensities. Thus, the analysis reveals several facts similar to the cases of KCl and KBr: The existence of a prominent positive peak on the DTR spectra around 12 eV is due to the large absorption peak around 10 eV; and the fine structures A , B , C , and D are the longitudinal counterparts of the subsidiary structures e , e' , f , and g , respectively. The longitudinal counterpart of the main peak d at 9.5 eV seems to exist at about 10 eV which is beyond the present measurements. These assignments of transverse-longitudinal splittings are tabulated numerically in Table V and indicated by pairs of vertical lines in Fig. 14. Theoretical plasmon energy to be observed is calculated and indicated at the bottom of Table V.

For the three potassium halides, a separation between the main absorption peak and the main DTR peak can be termed by a total longitudinal-transverse splitting between the large absorption peak and the DTR positive peak. The splittings for KCl, KBr, and KI are obtained as large as 1.3, 1.8, and 2.4 eV, respectively. The tendency for an increase in the splitting from KCl to KI

TABLE V. Energy positions of longitudinal and transverse structures in KI (in eV). Letters in the table similarly mean those in the Table I.

Absorption	Present study			Oscillators
	DTR	$\hbar\omega_{LT}$	EEL ^a	
<i>d</i> 9.5 <i>p</i>				9.4
<i>e</i> 10.3 <i>s</i>	<i>A</i> 10.7 <i>s</i>	0.4	10.1 <i>s</i>	10.3
<i>e'</i> 10.9 <i>s</i>	<i>B</i> 11.5 <i>s</i>	0.6	10.6 <i>s</i>	10.9
<i>f</i> 11.3 <i>s</i>	<i>C</i> 11.9 <i>mp</i>	0.6	11.9 <i>p</i>	11.3
<i>g</i> 12.3 <i>s</i>	<i>D</i> 12.6 <i>s</i>	0.3		12.4
<i>h</i> 13.4 <i>p</i>	<i>E</i> 13.8 <i>s</i>	0.4	13.8 <i>s</i>	
<i>i</i> 15.2 <i>p</i>	<i>F</i> 15.5 <i>p</i>	0.3	15.5 <i>p</i>	
<i>j</i> 16.2 <i>p</i>	<i>G</i> 16.6 <i>p</i>	0.4	16.5 <i>p</i>	
Theoretical	n_{eff}	$\hbar\omega_p$	$\hbar\omega_{obs}^b$	
	6.0	9.75	11.6 ($\hbar\omega_g = 6.3$)	
	6.4	10.1	11.9	

^aReferences 10 and 12.

^bReference 29.

can be explained by terms of the increase of the oscillator strength for the absorption peak in the same manner. The numerical parameters of the Lorentz model used in the three halides support the explanation.

IV. SUMMARY AND CONCLUSION

High-resolution longitudinal excitation spectra of three halides KCl, KBr, and KI in their plasmon regions were investigated by using oblique-incidence absorption spectroscopy with polarized VUV synchrotron radiation. Absorption spectra of these halides at both room and liquid-nitrogen temperatures were also measured in rather high resolution in 10–20 eV region for comparison. A prominent positive peak was demonstrated in the differential transmission ratio (DTR) spectra for various

angles of incidence at the higher energy side of a large interband absorption peak in each halide. Fine structures superimposed on the positive peak were discovered in each halide. This discovery not only improved and refined the previous work of the present author in KCl and KBr but also made it possible to reveal the complete interrelations between the transverse absorption spectrum and the longitudinal spectrum in these halides. For the analysis of the interrelations, the Lorentz oscillator model was applied, and the experimental results of DTR and absorption spectra were well reproduced by the calculation based on the model.

Exact calculations of the transverse and longitudinal spectra using available optical constants as well as the Lorentz model calculations confirmed that the positive peak in the DTR spectra and the loss function peak nearly completely correspond to each other in their profile and energy positions. Thus, the phenomenological origins of the positive peak in the DTR spectra or of the loss function peak in the three halides were given as follows.

(1) For the appearance of the plasmon loss peak, it is essential that a fairly large transverse absorption peak exists in the energy region where the oscillator strength of valence electron is mostly exhausted, but not necessarily completely exhausted.

(2) The profile of the plasmon peak is predominantly influenced by the fine structure located at the high-energy side of the absorption peak. The respective fine structure on the plasmon peak is the longitudinal counterpart of the transverse main peak and its fine structure.

(3) The total longitudinal-transverse splitting is affected by the oscillator strength for the absorption peak and, furthermore, the longitudinal peak (plasmon) is appreciably shifted toward higher energy by the influence of the existence of the fine structure on the high-energy of the transverse absorption peak.

Those statements may apply in other alkali halides and insulators as general properties. Each of these other substances, however, must have other unique properties.

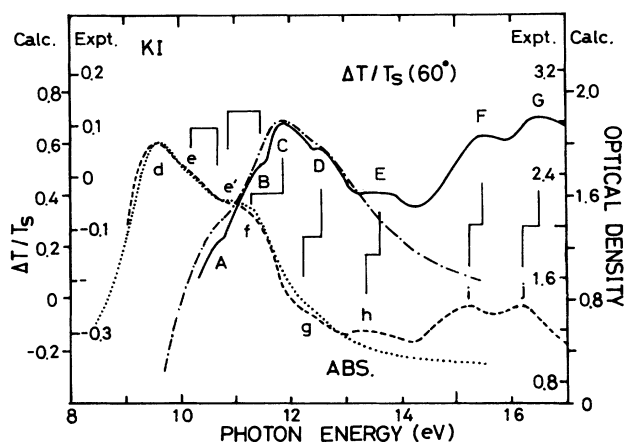


FIG. 14. Comparison between the experimental results and the Lorentz model calculations (five oscillators) in KI. DTR (60°), experimental, —; calculated, - - - - . Absorption spectra, experimental, — — —; calculated, ····. Pairs of vertical lines indicate longitudinal-transverse pairs for the experimental results. Thickness of specimen is 600 \AA for the calculated optical density curve and 150 \AA for the calculated optical density curve and 150 \AA for the calculated DTR.

TABLE VI. Numerical parameters of the oscillators fitted to the observed spectra in KI.

Oscillators	E (eV)	γ (eV)	σ	ϵ_0
1	9.4	1.3	23	
2	10.3	1.2	4.4	
3	10.9	0.9	2.3	$1.0+0.1i$
4	11.3	0.9	2.5	
5	12.4	1.0	0.5	

The above three statements also mean that the present results qualitatively support the Miyakawa's prediction concerning the existence of the plasmon in alkali halides as well as Horie's prediction.

Finally, the plasmon in the alkali halides differs remarkably from the one in the free-electron-like metals. This may be due to a large difference in the oscillator strength of the interband transitions, or in other words, of the longitudinal-transverse splitting between them.

ACKNOWLEDGMENTS

The author would like to express his gratitude to Professor O. Sueoka of the University of Tokyo for his kind help in the measurement of OIAS and for his critical reading of the manuscript, to Professor M. Watanabe of the Institute for Molecular Science and to Professor S. Sato of National Laboratory for High Energy Physics

(KEK) for their kind help in the measurement of the transverse absorption spectra. He also would like to express his thanks to the staff of Electron Synchrotron (ES) of the Institute for Nuclear Study (INS) for their kind operation of ES, and to the staff of the Synchrotron Radiation Laboratory, Institute of Solid State Physics (SRL-ISSP) for their generous assistance.

APPENDIX: LOSS FUNCTION OF MULTIOSCILLATOR

By using the Lorentz formula given by Eq. (4), the real and imaginary parts of dielectric parameter, ϵ_1 and ϵ_2 , respectively, and loss function $\text{Im}(-1/\epsilon)$ for a single oscillator ($m=1$, $\epsilon_0=1$) are as follows:

$$\epsilon_1(E) = 1 + \frac{\sigma_1(E_1^2 - E^2)}{(E_1^2 - E^2)^2 + \gamma_1^2 E^2}, \quad (\text{A1})$$

$$\epsilon_2(E) = \frac{\sigma_1 \gamma_1 E}{(E_1^2 - E^2)^2 + \gamma_1^2 E^2}, \quad (\text{A2})$$

$$\text{Im}(-1/\epsilon) = \frac{\sigma_1 \gamma_1 E}{[(E_1^2 - E^2) + \sigma_1]^2 + \gamma_1^2 E^2}. \quad (\text{A3})$$

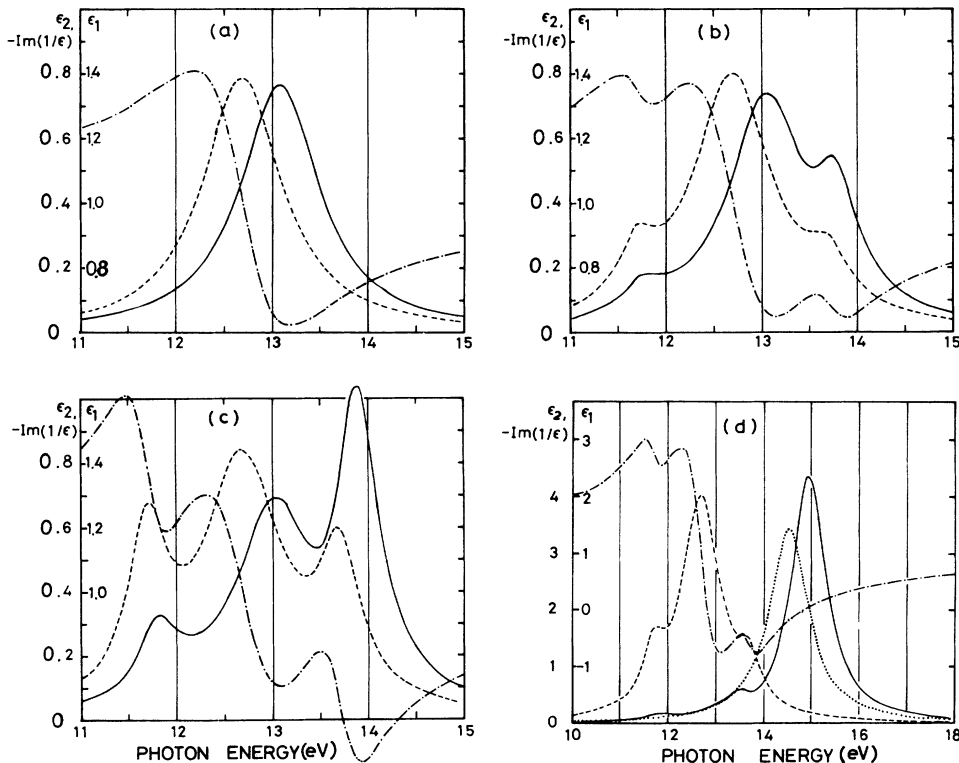


FIG. 15. Curves of the dielectric parameters: ϵ_1 (---), ϵ_2 (---), and the loss function $-\text{Im}(1/\epsilon)$ (—) for a single oscillator (a) ($\sigma=18$ and $\gamma=1$ eV); and for three-oscillator models (b) ($\sigma_2=18$ and $\sigma_1=\sigma_3=1$), (c) ($\sigma_2=18$ and $\sigma_1=\sigma_3=3$), and (d) ($\sigma_2=50$ and $\sigma_1=\sigma_3=5$). A dotted line in (d) indicates a loss function for the single main oscillator.

Numerical calculations of (A1)–(A3) are performed for values $E_1=12.7$ eV, $\sigma_1=18$ and $\gamma_1=1$ eV that are expected to reproduce closely the experimental absorption intensity in KCl. In Fig. 15(a) are shown the results of the calculation. The longitudinal-transverse (L-T) splitting is found to be about 0.4 eV. Next, three oscillators are taken ($m=3$, $\epsilon_0=1.0$) in which $n=2$ is the main oscillator and the remaining two ($n=1$ and 3) are small subsidiaries located 1 eV distant from the main oscillator, one on the high-energy side and one on the low. Two cases for the three-oscillator system are illustrated in Figs. 15(b) and 15(c). In the case of 15(b), $\sigma_1=\sigma_3=1$, $\sigma_2=18$, $\gamma_1=\gamma_3=0.5$ eV, and $\gamma_2=1$ eV. In the case of Fig. 15(c), $\sigma_1=\sigma_3=3$, and the others are same as in 15(b). Lastly, similar calculations are performed on a condition that σ_2 is very large ($\sigma_2=50$, $\sigma_1=\sigma_3=5$), but that other values are same as in 15(b) or 15(c). Results of these calculations are illustrated in 15(d). The L-T splitting of the main oscillator in the last case is about 2.2 eV which is much bigger than those in the other three cases.

From these calculations and results of the typical four cases the following facts are confirmed.

(1) When the intensity of the main oscillator is appropriate, the longitudinal peak corresponding to a higher energy subsidiary oscillator is remarkably

enhanced whereas a lower energy one is suppressed, and the L-T splitting is larger for the higher energy band than the lower energy band.

(2) When the main oscillator has a much larger intensity, the L-T splitting of the main peak is very large, whereas the longitudinal counterparts of both subsidiary oscillators have very small intensities and L-T splittings.

(3) The intensity and profile of ϵ_2 for multioscillators are additionally determined from those for each oscillator, but intensity and profile of $\text{Im}(-1/\epsilon)$ are not additional.

From fact (1), it can be said that the longitudinal counterparts of the subsidiary oscillators located at slightly higher energy from the main oscillator determine the dominant profile of the loss peak, whereas the longitudinal counterpart of the main oscillator contributes weakly to it. This tendency reflects the character of rapidly changing dielectric parameters in the energy region. The case noted in fact (2) does not fit the present experimental results and rather corresponds to the phenomena in the free-electron-like metals. Fact (3) indicates that in the oscillator model, either the peak in the loss function spectrum or the positive peak in the DTR spectrum cannot be divided into components which contribute to the formation of the peak.

¹H. R. Philipp and H. Ehrenreich, *Phys. Rev.* **131**, 2016 (1963).

²D. M. Roessler and W. C. Walker, *Phys. Rev.* **166**, 599 (1968).

³G. Stephan, E. Garignon, and S. Robin, *C. R. Acad. Sci. Paris* **268**, 408 (1969); G. Stephan and S. Robin, *Opt. Commun.* **1**, 40 (1969).

⁴A. Ejiri, M. Watanabe, H. Saito, H. Yamashita, T. Shibaguchi, H. Nishida, and S. Sato, *Digest of the 3rd International Conference on Vacuum-Ultraviolet Physics*, Tokyo, 1971, edited by Y. Nakai (Physical Society of Japan, Tokyo, 1971).

⁵G. W. Rubloff, J. Freeouf, H. Fritzsche, and K. Murase, *Phys. Rev. Lett.* **26**, 1317 (1971); G. W. Rubloff, *Phys. Rev.* **135**, 662 (1972).

⁶M. Antinori, A. Balzarotti, and M. Piacentini, *Phys. Rev. B* **7**, 1541 (1973).

⁷H. Overhof, *Phys. Rev. B* **5**, 4079 (1972).

⁸T. C. Collins, A. B. Kunz, and J. T. Devreese, *Int. J. Quantum Chem. Symp. No. 7*, 551 (1973).

⁹O. Sueoka, *J. Phys. Soc. Jpn.* **19**, 2239 (1964); **20**, 2226 (1965).

¹⁰M. Creuzburg and H. Raether, *Solid State Commun.* **2**, 175 (1964).

¹¹P. Keil, *Z. Naturforsch.* **21A**, 503 (1966); *Z. Phys.* **214**, 226 (1968).

¹²M. Creuzburg, *Z. Phys.* **196**, 433 (1966).

¹³J. Gieger, P. Odelga, and H. Chr. Pfeiffer, *Phys. Status Solidi* **15**, 531 (1966).

¹⁴C. Gout and F. Pradal, *J. Phys. Chem. Solid* **29**, 581 (1968).

¹⁵D. W. Berreman, *Phys. Rev.* **130**, 2193 (1963).

¹⁶A. Ejiri, *Sci. Light (Toyko)* **26**, 1 (1977).

¹⁷A. Ejiri, *J. Phys. Soc. Jpn.* **44**, 565 (1978).

¹⁸A. Ejiri, *J. Phys. Soc. Jpn.* **23**, 901 (1967).

¹⁹A. Ejiri, *J. Phys. Soc. Jpn.* **24**, 1181 (1968).

²⁰Preliminary results have been reported on the paper, A. Ejiri, J. C. Lemonnier, and O. Sueoka, *Ann. Isr. Phys. Soc.* **6**, 267 (1984).

²¹G. Stephan, theses, University of Rennes, 1970.

²²M. Piacentini, C. G. Olson, and D. W. Lynch, *Phys. Rev. Lett.* **35**, 1658 (1975).

²³See, for example, F. Stern, in *Solid State Physics*, edited by F. Seitz and D. Turnbull (Academic, New York, 1963), Vol. 15, p. 229.

²⁴In the formulas similarly given by the present author in Refs. 16 and 17, the expressions T_p and T_s must be replaced by t_p and t_s , respectively.

²⁵A. Ejiri and O. Sueoka in *Proceedings of the International Conference on X-ray and Vacuum-Ultraviolet Synchrotron Radiation Instrumentation*, Stanford, 1985, edited by G. S. Brown and E. I. Lindau (North-Holland, Amsterdam, 1986), p. 283; *Nucl. Instrum. Methods Phys. Res. A* **246**, 282 (1986).

²⁶For details, please refer to the paper by M. Watanabe, A. Ejiri, H. Yamashita, H. Saito, S. Sato, T. Shibaguchi, and H. Nishida, *J. Phys. Soc. Jpn.* **31**, 1085 (1971).

²⁷J. E. Eby, K. J. Teegarden, and D. S. Dutton, *Phys. Rev.* **116**, 1099 (1959).

²⁸D. M. Roessler and W. C. Walker, *J. Opt. Soc. Am.* **58**, 275 (1968).

²⁹C. Hoire, *Prog. Theor. Phys.* **21**, 113 (1959).

³⁰T. Miyakawa, *J. Phys. Soc. Jpn.* **24**, 768 (1968).